© 2016. Published by The Company of Biologists Ltd | Development (2016) 143, 2172-2182 doi:10.1242/dev.133678

RESEARCH ARTICLE

Fat3 and Ena/VASP proteins influence the emergence of asymmetric cell morphology in the developing retina

Alexandra Krol, Steven J. Henle and Lisa V. Goodrich*

ABSTRACT

Neurons exhibit asymmetric morphologies throughout development – from migration to the elaboration of axons and dendrites – that are correctly oriented for the flow of information. For instance, retinal amacrine cells migrate towards the inner plexiform layer (IPL) and then retract their trailing processes, thereby acquiring a unipolar morphology with a single dendritic arbor restricted to the IPL. Here, we provide evidence that the Fat-like cadherin Fat3 acts during multiple stages of amacrine cell development in mice to orient overall changes in cell shape towards the IPL. Using a time-lapse imaging assay, we found that developing amacrine cells are less directed towards the IPL in the absence of Fat3, during both migration and retraction. Consistent with its predicted role as a cell-surface receptor, Fat3 functions cell-autonomously and is able to influence the cytoskeleton directly through its intracellular domain, which can bind and localize Ena/VASP family actin regulators. Indeed, a change in Ena/VASP protein distribution is sufficient to recapitulate the *Fat3* mutant amacrine cell phenotype. Thus, Fat-like proteins might control the polarized development of tissues by sculpting the cytoskeleton of individual cells.

KEY WORDS: Amacrine cell, Retinal development, Fat3, Ena/VASP, Planar polarity

INTRODUCTION

Mature neurons have polarized morphologies that enable the directional flow of information through circuits. Efforts to understand how this polarity is established have focused on axon specification (Barnes et al., 2008). However, many neurons exhibit asymmetries in the absence of an axon, exemplified by retinal amacrine cells. Additionally, developing neurons exhibit directed behaviors before axons emerge. At each stage, a precisely organized cytoskeleton lies at the heart of a neuron's functional and morphological asymmetry. Although it is well-established that regulation of actin and microtubules can influence neuronal polarity, it remains unclear how such intrinsic changes are coordinated with the surrounding tissue such that neurons and their processes are correctly positioned.

In other tissues, polarized cells are organized with respect to each other and the surrounding cells by planar polarity pathways. This type of organization is typified in the fly wing, where bristles point in a common direction (Devenport, 2014). Two systems for planar polarity have been described: the core planar cell polarity (PCP) pathway and the Fat/Dachsous system (Sopko and McNeill, 2009). In both cases, the key players are asymmetrically localized and affect both the intracellular polarity of a cell and its ability to propagate polarity information to its neighbors. These systems are conserved in vertebrates, where they induce and coordinate asymmetries throughout the body. However, in the nervous system, planar polarity signaling influences cellular behaviors that are not obviously polarized within the plane of an epithelium, such as collective cell migration and axon guidance (Goodrich and Strutt, 2011). Thus, although mutations in planar polarity genes lead to major defects in brain organization and function, the cellular origins of these phenotypes are often unclear.

Previously, we showed that the Fat-related protein Fat3 is required for neuronal morphogenesis (Deans et al., 2011). In the retina, amacrine cells project a single dendritic arbor into the inner plexiform layer (IPL), a layer of neuropil that separates cell bodies in the inner nuclear layer (INL) from those in the ganglion cell layer (Fig. 1A). In *Fat3* mutant mice, many amacrine cells form a second projection that is directed away from the IPL (Fig. 1B), creating two ectopic synaptic layers in the mature retina. Although the final consequences are dramatic, it remains unknown how Fat3 normally prevents amacrine cells from extending extra dendrites. Counterintuitively, Fat3 protein is asymmetrically localized to amacrine cell processes in the IPL, i.e. opposite to where the extra neurites form. This raises the possibility that, like more familiar polarity proteins, Fat3 might transmit a local signal that influences cytoskeletal organization across the neuron.

Fat3 is one of four Fat-related genes in the mammalian genome, *Fat1-Fat4*, which all encode single-pass transmembrane proteins with large extracellular domains and unstructured intracellular domains of ∼400 amino acids. *Fat4* is the vertebrate ortholog of *Drosophila fat* and *Fat1-Fat3* share greater sequence similarity with *Drosophila fat-like* (Tanoue and Takeichi, 2005). Whereas Fat4 plays a conserved role in planar polarity (Saburi et al., 2008), little is known about how Fat-like proteins might influence cell shape and orientation in any system (Sadeqzadeh et al., 2014), with only a handful of possible polarity phenotypes described in either flies (Viktorinova et al., 2009) or vertebrates (Caruso et al., 2013; Le Pabic et al., 2014; Saburi et al., 2012).

At the molecular level, Fat-related proteins are poised to mediate direct effects on the organization of the cytoskeleton. For instance, Fat aligns microtubules along the proximo-distal axis of the fly wing (Harumoto et al., 2010; Matis et al., 2014) and Fat-like orients actin filaments in follicular cells (Viktorinova et al., 2009). Mammalian Fat1 can affect actin organization *in vitro*, at least in part by localizing Enabled/Vasodilator-stimulated phosphoprotein (Ena/VASP) proteins through binding sites in its intracellular domain (Moeller et al., 2004; Tanoue and Takeichi, 2004). Ena/VASP proteins are regulated by recruitment to the plasma membrane, where they promote formation of filamentous actin (Bear and Gertler, 2009; Krause et al., 2003) and hence influence cell migration, as well as the initiation and extension of neuronal

Department of Neurobiology, Harvard Medical School, Boston, MA 02115, USA.

*Author for correspondence (Lisa_Goodrich@hms.harvard.edu)

L.V.G., 0000-0002-3331-8600

Received 1 December 2015; Accepted 14 April 2016

Development (2016) 143, 2172-2182 doi:10.1242/dev.133678

processes (Dent et al., 2007; Kwiatkowski et al., 2007; Lebrand et al., 2004). This raises the possibility that Fat3 works together with Ena/VASP proteins to organize the actin cytoskeleton in amacrine cells.

To learn how intrinsic changes in neuron shape are coordinated with the environment, we investigated the roles of Fat3 and Ena/VASP proteins in amacrine cells as they develop in the natural environment of the retina. Our evidence suggests that Fat3 acts autonomously to guide overall asymmetries in amacrine cell behaviors that precede the appearance of extra dendrites, possibly acting through Ena/VASP effectors.

RESULTS

Fat3 is required for directed migration of amacrine cells

Since Fat3 is localized to processes in the IPL (Deans et al., 2011), we hypothesized that Fat3 propagates an overall change in cytoskeletal organization, echoing the effects of other Fat-related proteins on tissue polarity. In support of this idea, phalloidin staining revealed that F-actin was strongly enriched in the IPL of control retinas at postnatal day (P)11 (Fig. 1C), but this distribution was shifted outside the IPL in *Fat3* mutants (Fig. 1D). Fat3 can be detected in the IPL as soon as it forms (Deans et al., 2011), raising the possibility that this defect in mature amacrine cell morphology reflects an earlier role for Fat3 in the control of the cytoskeleton. Developing amacrine cells undergo rapid and transient changes in cytoskeletal organization that manifest as changes in cell shape. Thus, we developed a time-lapse imaging assay that allowed us to visualize individual amacrine cell precursors and track their overall dynamics as they transition from migratory bipolar morphologies to their mature unipolar morphology *in situ*.

Because amacrine cells are produced over a broad window of time, the developing retina contains precursors at many stages of development (Hinds and Hinds, 1978, 1983; Voinescu et al., 2009). In order to track a temporally defined subset as they progress through these stages, we labeled a cohort of late-born amacrine cell precursors by electroporating a Cre-dependent plasmid encoding myristoylated-Venus (*fsf-memVenus*) into P0 $Fat3^{fl/+}$ or $Fat3^{fl/-}$ pups harboring the *Ptf1a-Cre* transgene, which is active in all amacrine cells. By using *Ptf1a-Cre* to create conditional knock-out mice ($Fat3^{cKO}$) for all of our studies, we were able to focus on the amacrine cell-specific activities of Fat3 and avoid potential confounds from its apparent role in ganglion cells (Deans et al., 2011). This approach clearly revealed the morphology of individual amacrine cells, which projected strictly

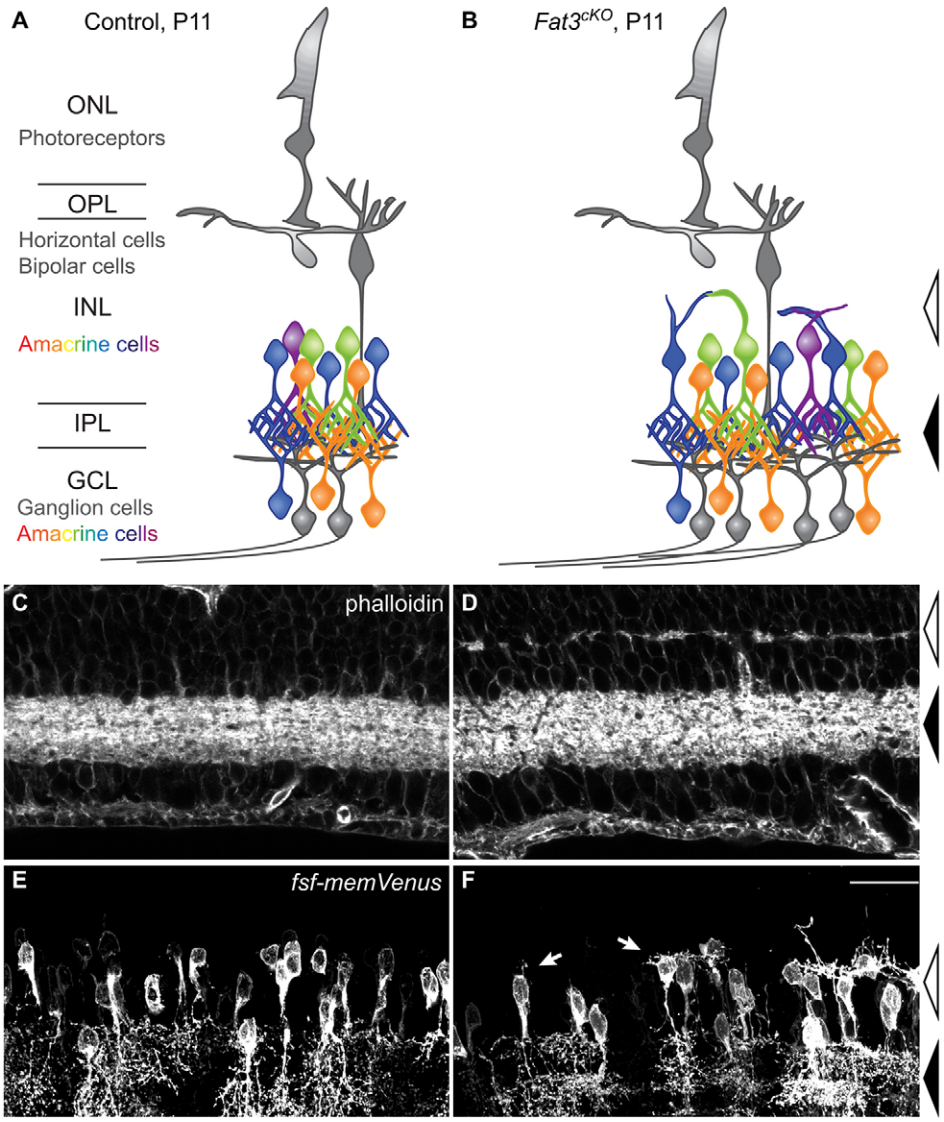

Fig. 1. Loss of Fat3 leads to changes in global actin distribution. (A,B) Retinal organization in control (A) and $Fat3^{cKO}$ (B) animals at P11. Retinal neurons reside in three cellular layers (ONL, INL and GCL) separated by two layers of neuropil (OPL, IPL). Amacrine cells in the INL and GCL normally elaborate a single dendritic arbor restricted to the IPL (black arrowhead). In $Fat3^{cKO}$, some amacrine cells extend additional processes away from the IPL, forming an ectopic plexiform layer (white arrowhead). Colors represent the large number of amacrine cell subtypes born across development. (C,D) Phalloidin labeling of filamentous actin (F-actin) in mature, P11 retinas from control (C) and $Fat3^{cKO}$ (D) animals. Whereas F-actin is usually enriched only in the IPL (black arrowhead), extra actin accumulates ectopically in the INL of *Fat3* mutant retina (white arrowhead). Similar results were observed in multiple samples at P6 and P11. (E,F) Confocal images of late-born amacrine cells at P11 that were labeled by electroporation at P0 with *Ptf1a-Cre*-dependent expression of membrane-localized Venus (*fsf-memVenus*). Control amacrine cells (E) develop normal unipolar morphologies. Late-born amacrine cells often develop extra processes (arrows) in $Fat3^{cKO}$ mutants (F). Scale bar: 30 µm in F for C-F. GCL, ganglion cell layer; INL, inner nuclear layer; IPL, inner plexiform layer; ONL, outer nuclear layer; OPL, outer plexiform layer.

Development (2016) 143, 2172-2182 doi:10.1242/dev.133678

into the IPL in control retinas at P11 (Fig. 1E). By contrast, memVenus-labeled *Fat3*^{cKO} amacrine cells extended neurites away from the IPL and contributed to an ectopic layer of neuropil (Fig. 1F), with at least 18% and up to 80% of labeled cells affected across regions analyzed (n=12 regions across four animals). Thus, late-born amacrine cells, like many other subtypes (Deans et al., 2011), require Fat3 for normal development.

To visualize the cellular dynamics that occur as late-born amacrine cells assume their morphologies, we electroporated dissected retinas with *fsf-tdTomato* at P0, cultured them for 1 day, and captured images every 20 min for 16-24 h using a two-photon confocal microscope. Unexpectedly, this approach revealed that leading processes are present in the IPL even while their cell bodies are still close to the outer limiting membrane. This suggests that the leading processes of migrating amacrine cell precursors contribute to the Fat3 immunolabeling observed in the nascent IPL (Deans et al., 2011). Thus, Fat3 might act much earlier than expected. Indeed, time-lapse imaging showed that migrating *Fat3*^{cKO} and control amacrine cells followed significantly different trajectories. Whereas control amacrine cell bodies moved in a smooth, progressive fashion towards the IPL (Fig. 2A, Movie 1) (n=3 movies), *Fat3*^{cKO} amacrine cells often moved in the opposite direction (Fig. 2B, Movie 2) (n=3 movies). We visualized these differences by plotting the position of each cell over time, normalized to its lowest position over the course of imaging (Fig. 2A′,B′), and found that an erratic pattern of migration was present across the population, as illustrated by overlaying the trajectories for all wild-type (n=75) and mutant (n=75) amacrine cells (Fig. S1). Quantification confirmed that mutant cells vacillated, changing direction significantly more frequently than control cells (Fig. 2C). There was also a significant difference in the distribution of net migration rates, with *Fat3*^{cKO} amacrine cells often taking longer to reach the IPL (Fig. 2D). Individual instantaneous movements were actually faster (Fig. 2E), confirming that the phenotype is not due to impaired motility per se.

To assess the cumulative effect on migration, cell body position was measured relative to the IPL (Fig. 3A-C). As predicted by the analysis of net migration rates (Fig. 2D), *Fat3* mutant cell bodies were positioned farther away from the IPL after 48 h *in vitro*, as determined by counting the number of labeled cells present in each of three bins spanning the INL (yellow lines, Fig. 3A,B). To determine whether migration was also delayed *in vivo*, we collected retinas from *Ptf1a-Cre; AI14(tdTomato* reporter*)* pups and examined the distribution of all amacrine cells at P1, when most early-born amacrine cells have completed migration and therefore reside in the bottom third of the INL (Fig. 3D-G). Indeed, significantly more labeled amacrine cells were still in the middle third of the mutant retina (bin 2) compared with controls (Fig. 3D,E, with enlarged views of bin 2 shown in 3D′,E′), such that the overall distribution was shifted away from the IPL (Fig. 3G). Thus, in the

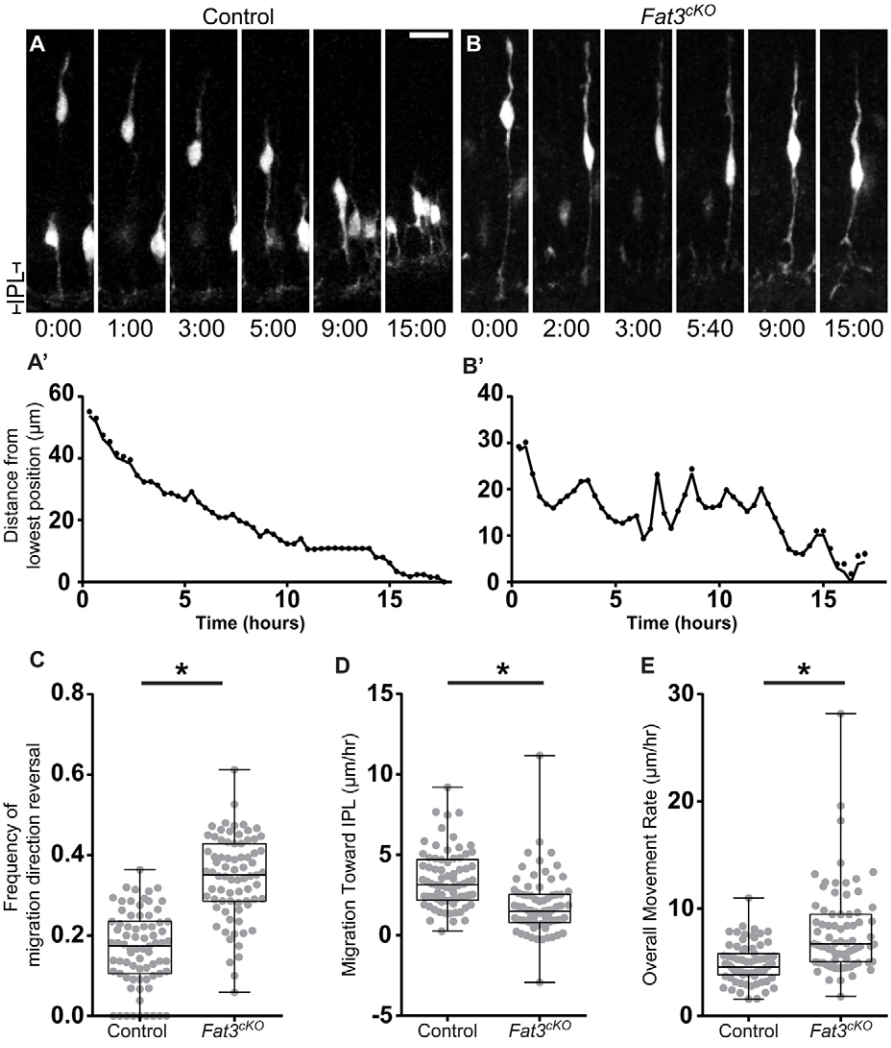

Fig. 2. Amacrine cell migration is less directional in the absence of Fat3. (A,B) Representative time-lapse images of developing amacrine cells in organotypic slice cultures of P0 retinas from control (A) and *Fat3*^{cKO} (B) animals. In controls, the cell body progresses smoothly towards the IPL over 15 h (hh:mm). In *Fat3*^{cKO} mutants, the cell body often reverses direction and makes less progress towards the IPL. For each movie, cell body position was plotted over time and normalized to the lowest point reached during the imaging period (A′,B′). See Fig. S1 for tracks of all analyzed cells. Scale bar: 20 µm in A for A,B. (C-E) Quantitative analysis of amacrine cell migration. Cells were tracked in the middle third of the retina. Compared with controls, *Fat3*^{cKO} amacrine cells change direction more frequently (C). The distribution of net migration rates towards the IPL was significantly different (D), with mutant amacrine cells appearing to take longer overall despite making faster instantaneous movements (E). n=75 cells for each condition from three control and five *Fat3*^{cKO} animals. *P<0.0001, Mann–Whitney U-test. In this and all following figures, boxplots show median and interquartile range; whiskers indicate range. Raw data plotted in gray.

Development (2016) 143, 2172-2182 doi:10.1242/dev.133678

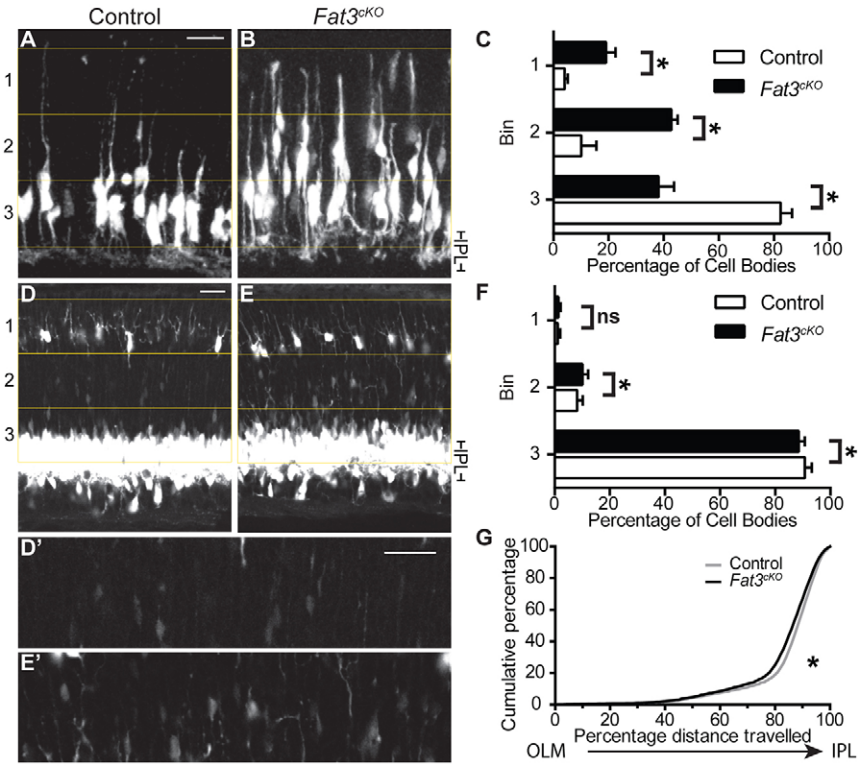

Fig. 3. Cumulative migration of amacrine cells is delayed with loss of Fat3. (A-C) Representative images of a cohort of late-born amacrine cells electroporated at P0, and then cultured for 48 h in a retinal slice culture. Many more migrating cells are still in the middle third of the retina (bin 2) in *Fat3*^{cKO} mutants (B) compared with controls (A), as quantified in C (n=3 control, and n=5 *Fat3*^{cKO} movies, from Fig. 2). Scale bar: 20 µm. *P<0.01, t-test; bin 1, P=0.002; bin 2, P=0.0006; bin 3, P=0.0004. Bars show mean±s.d. (D,E) Representative images of P1 retinas from control (D) and *Fat3*^{cKO} (E) animals; for each retina (n=4 per condition), images were collected from four different regions within 500 µm of the optic nerve. Amacrine cells were labeled genetically using *Ptf1a-Cre* combined with a tdTomato reporter. Horizontal cells at the top of the INL were also labeled. High-power views of the boxed regions highlight the increased number of amacrine cells in the middle third (bin 2) of the mutant retina (E′) compared with the control (D′). Scale bar: 30 µm in D,D′ for D-E′. (F) Quantification of amacrine cell position confirmed a significant increase in the percentage of amacrine cells in the middle third, with a corresponding decrease in the percentage that had reached the bottom third by P1. *P<0.01, t-test; bin 1, P=0.52; bin 2, P=0.01; bin 3, P=0.01. Bars show mean±s.d. (G) A cumulative histogram of the distribution of amacrine cells confirms a significant shift away from the IPL in *Fat3*^{cKO} mutants. *P<0.0001, Kolmogorov–Smirnov test. ns, not significant.

absence of Fat3, cells no longer migrate directly towards the IPL and take longer to reach the bottom of the INL.

Fat3 promotes differential behavior of the trailing and leading neurites

Although time-lapse imaging indicated a defect in IPL-directed migration, most *Fat3* mutant amacrine cells ultimately reach the appropriate position, leaving it unclear how this early change in behavior is related to the retention of extra processes observed at P11. To address this issue, we imaged amacrine cell precursors slightly later, as they finish migrating and begin to retract their trailing processes. Control neurites retracted in a relatively smooth fashion (Fig. 4A, Movie 3), much like the migration of the cell body one day earlier. By contrast, trailing neurites of *Fat3* mutant cells often re-extended (Fig. 4B, between 5 and 6 h, 7 and 10 h; Movie 4) and had a significantly slower net retraction rate (Fig. 4C). Overall, 33% of *Fat3*^{cKO} amacrine cells (n=42 cells, n=5 movies) had negative trailing process retraction rates, which means that their trailing processes lengthened rather than retracted over the course of imaging. However, only 6% of control cells (n=49 cells, three movies) showed net extension. Similar to what was observed for migrating precursors, the tips of the trailing neurites moved faster in *Fat3* mutants (Fig. 4D). Unexpectedly, *Fat3*^{cKO} trailing neurites also branched frequently and branches sometimes even emerged aberrantly from the cell body (Fig. 4E, Movie 5). In control amacrine cells, only 12% showed branching events outside of the leading neurite over the course of imaging (n=50 cells, n=3 movies). By contrast, 70% of *Fat3*^{cKO} cells (n=40 cells, n=5 movies) showed frequent episodes of ectopic branching in the trailing process or cell body. Quantification confirmed *Fat3*^{cKO} neurons had a significantly higher branching index, a metric that reflects both the number and duration of branches (see Materials and Methods) (Fig. 4F).

Altogether, time-lapse imaging demonstrated that amacrine cells normally migrate in a directed fashion and that this axis is mirrored in the behavior of the neurites. In *Fat3*^{cKO} amacrine cells, the pattern of cellular dynamics is no longer biased towards the IPL, leading first to erratic migration and then erratic retraction and branching of the trailing processes. These changes in cellular dynamics suggest that Fat3 normally influences the overall pattern of cytoskeletal organization in developing amacrine cells.

Fat3 can have cell-autonomous effects on amacrine cell polarity

Next, we asked how Fat3, which is a transmembrane protein localized to the leading process, is able to induce overall changes in cell morphology. One simple model is that Fat3 mediates its effects directly, detecting a cue in the IPL through its extracellular domain and transmitting this information to the cytoskeleton through its intracellular domain (ICD). Indeed, *Drosophila* Fat has clear effects on microtubule alignment (Harumoto et al., 2010; Matis et al., 2014) and mammalian Fat1 can bind to known actin regulators and influence actin organization *in vitro* (Moeller et al., 2004; Tanoue and Takeichi, 2004). However, in flies, *fat-like* has non-autonomous effects, with only large loss-of-function clones showing a polarity phenotype (Viktorinova et al., 2009), and *fat* has also been proposed to act non-autonomously through expression of a secreted molecule (Fanto et al., 2003; Sopko and McNeill, 2009). Similarly, Fat3 could influence amacrine cell morphologies by altering the activity or distribution of a secreted factor in the IPL.

To determine whether Fat3 can act autonomously, *Fat3* was removed from a sparse population of late-born amacrine cells by electroporating *Cre* into *Fat3*$^{fl/-}$ retinas, along with the *fsf-memVenus* reporter (to visualize morphology) and an *Ndrg4* fluorescent reporter plasmid (to identify amacrine cells independent of any changes in morphology) (Cherry et al., 2009) (Fig. 5A,B). Under these conditions, development proceeded unperturbed until P0, when *Fat3* was removed from a small number of amacrine cells (i.e. *Fat3*^{cKO}) developing in an otherwise

Development (2016) 143, 2172-2182 doi:10.1242/dev.133678

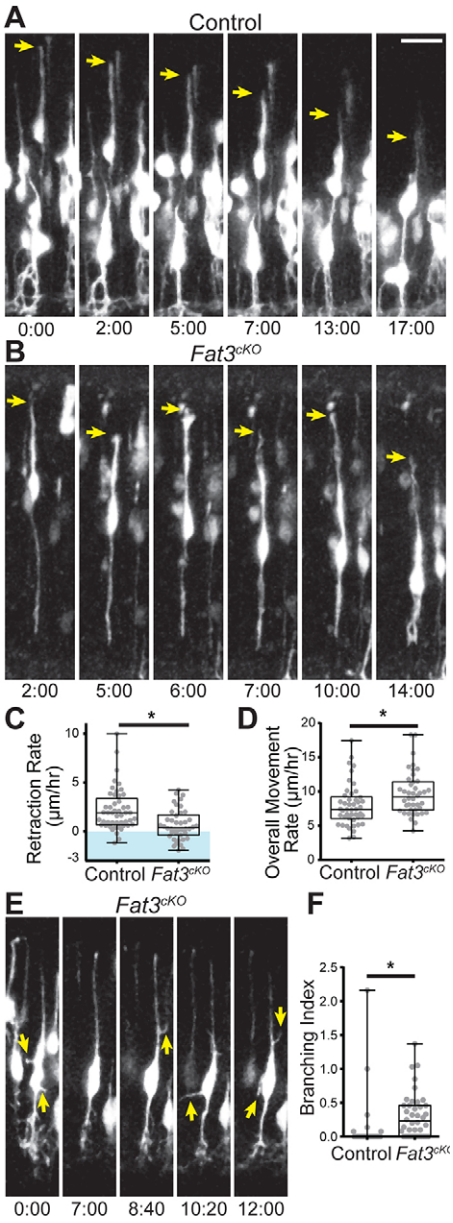

Fig. 4. Trailing neurite dynamics are altered in *Fat3* mutants.
(A,B) Representative time-lapse images of developing amacrine cells in an organotypic slice culture highlighting trailing process retraction. Arrows indicate the tip of the trailing process tracked in control (A) and $Fat3^{cKO}$ (B) animals. Scale bar: 20 µm in A for A,B. (C,D) Quantification of trailing process behavior during development. The trailing process retraction rate (overall change in length/time) in $Fat3^{cKO}$ mutants (C) is significantly slower. Many cells have negative rates (shaded in blue) indicating net extension over the course of imaging. Nevertheless, in $Fat3^{cKO}$ mutants, the overall tip movement rate (absolute change in length between frames/time) is greater (D). (E) Representative series of time-lapse images illustrates aberrant branches extending from the trailing process and cell body of a $Fat3^{cKO}$ amacrine cell. (F) Quantification of branching frequency in control and $Fat3^{cKO}$ mutants. Branching index reflects the cumulative number of ectopic branches observed at each time point divided by the number of time points in the imaging session. Three control and five $Fat3^{cKO}$ animals. *P<0.01, Mann–Whitney U-test. In C, P=0.0001, n=49 cells for control and n=42 for $Fat3^{cKO}$. In D, P=0.004, n=46 cells for control and n=42 for $Fat3^{cKO}$. In F, P<0.0001, n=50 cells for control and n=40 for $Fat3^{cKO}$.

wild-type environment; $Fat3^{fl/+}$ animals were used as controls. Cells were analyzed by building three-dimensional reconstructions (Fig. 5A′,B′), which allowed us to measure the length of any non-IPL directed neurites emanating from $Ndrg4^{+}$ cells. We found that extra neurites developed in many Cre-electroporated $Fat3^{fl/-}$ cells, including in well-isolated cells (Fig. 5C,D). A cumulative distribution plot confirmed that control Cre-positive heterozygous amacrine cells rarely extended any processes away from the IPL. By contrast, the $Fat3^{fl/-}$ population was significantly shifted, with many more cells elaborating long neurites (Fig. 5E). To control for experimental variability, we determined the percentage of cells with extra neurites longer than 10 µm per electroporated region. Across regions, a significantly greater percentage of $Fat3^{fl/-}$ electroporated cells had extra neurites compared with the control (Fig. 5F). These results suggest that Fat3 acts cell-autonomously to influence amacrine cell shape.

Fat3 recruits Ena/VASP through a conserved binding site and alters its distribution *in vivo*

The ability of Fat3 to act cell-autonomously favors a model where Fat3 acts in the tip of the leading neurite to induce changes in cytoskeletal organization through its ICD. Although no Fat3 effectors have been defined, Fat3 is closely related to Fat1, which binds to Ena/VASP family members through two Ena/VASP homology (EVH1) sites in its ICD (Moeller et al., 2004; Tanoue and Takeichi, 2004). The Ena/VASP family of actin regulators comprises Mena, EVL and VASP, which play important roles in neurite elongation and neuronal migration, often acting redundantly (Dent et al., 2007; Goh et al., 2002; Kwiatkowski et al., 2007). Western blots confirmed that all three Ena/VASP family members are present throughout retinal development (Fig. 6A). Moreover, co-immunostaining demonstrated that although Mena is broadly expressed, there is enriched expression that overlaps with Fat3 in the nascent IPL at P0 (Fig. 6B) and at P6 (Fig. 6C), when most amacrine cells are unipolar. Therefore Ena/VASP proteins are expressed at the right time and in the right place to interact with Fat3 during amacrine cell development.

Analysis of the Fat3 intracellular domain (Fat3ICD) revealed three possible EVH1 binding sites, including two with conservation to the EVH1 binding sites in Fat1 (Fig. 7A). To test whether these sites can affect Ena/VASP distribution, we fused the Fat3ICD to Venus, preceded by a sequence that targets the protein to the mitochondria outer leaflet, a site typically devoid of Ena/VASP proteins (Fig. 7B). When expressed in COS-7 cells (Fig. 7C,D), the Fat3ICD strongly recruited endogenous VASP to mitochondria (Fig. 7C′,D′ and C″,D″). Moreover, a truncated construct lacking all three predicted binding sites (Fig. 7B) did not induce this change in distribution (Fig. S2). Analysis of additional deletion constructs revealed that the second EVH1 site is both necessary and sufficient for this effect; neither site 1 nor site 3 was required (Fig. 7B and Fig. S2). *In vitro* pulldown assays confirmed that the Fat3ICD bound VASP, EVL and Mena in neonatal brain lysate (Fig. 7E, Full, and data not shown); when all three sites were removed, this binding was lost (Fig. 7E, Trunc). Similarly, there was no interaction when the amino acid that is crucial for Ena/VASP binding was mutated to an alanine in the second site (Fig. 7E, Mut2). A point mutation in the first site had no effect (Fig. 7E, Mut1). Thus, the Fat3ICD can interact with Ena/VASP in both cellular and biochemical contexts. The interaction is likely to be direct because a point mutation in a predicted EVH1 binding site prevented binding of Ena/VASP proteins.

Consistent with these *in vitro* findings, Ena/VASP localization was disrupted in *Fat3* mutant retinas. In control P6 retinas, all three family members were broadly expressed yet concentrated in the IPL (Fig. 6C and Fig. 8A,C,E). However, in *Fat3* mutant retinas, Mena,

Development (2016) 143, 2172-2182 doi:10.1242/dev.133678

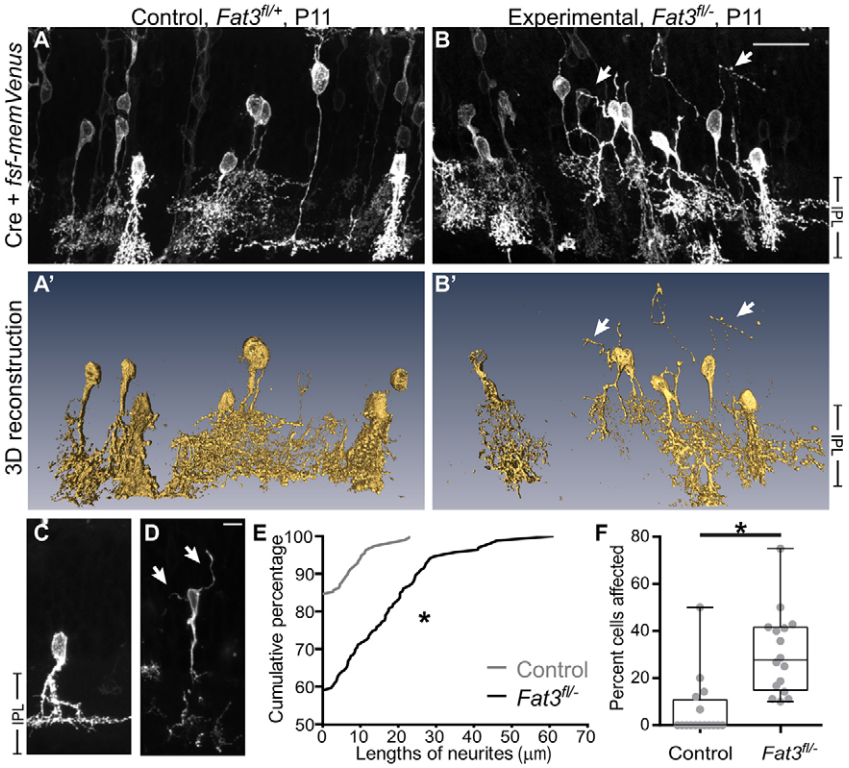

Fig. 5. Cell-autonomous loss of Fat3 disrupts amacrine cell morphology. (A,B) Confocal images of *Fat3*$^{fl/+}$ (A) and *Fat3*$^{fl/-}$ (B) retinas electroporated at P0 with plasmids expressing Cre and Cre-dependent memVenus. Cre-positive amacrine cells developed unipolar morphologies in controls but often extended extra neurites away from the IPL in *Fat*$^{fl/-}$ animals (arrows). Amacrine cell identities were confirmed independently by co-electroporation of a *Ndrg4* promoter-driven reporter, which marks amacrine cells at P11 (not shown). Three-dimensional reconstructions of each Ndrg4^{+} cell were created for quantification (A′,B′). Scale bar: 30 µm in B for A-B′. (C,D) Representative Cre^{+} amacrine cells illustrate the formation of extra processes in isolated *Fat*$^{fl/-}$ (D, arrows) but not control *Fat*$^{fl/+}$ (C) cells. Scale bar: 10 µm in D for C,D. (E) Cumulative histogram of lengths of all non-IPL facing neurites, measured in reconstructions of Cre-electroporated Ndrg4^{+} amacrine cells. **P*<0.0001, Kolmogorov–Smirnov test. (F) The percentage of cells with extra neurites greater than 10 µm in each electroporated region. *n*=16 different electroporated regions from four retinas for each genotype. **P*<0.0001, Mann–Whitney *U*-test.

VASP and EVL were mislocalized to a band running through the developing INL (Fig. 8B,D,F, arrowhead and insets). Therefore, Ena/VASP localization is altered in *Fat3* mutant retina, suggesting a mechanism by which Fat3 could affect the cytoskeletal organization of developing amacrine cells.

Uniform Ena/VASP localization phenocopies loss of Fat3

Mislocalization of Ena/VASP actin regulators could provide a molecular explanation for the *Fat3* mutant amacrine cell phenotype. Alternatively, the observed changes in Ena/VASP distribution could be secondary to the retention of actin-rich trailing neurites. To distinguish between these possibilities, we sought to change the distribution of endogenous Ena/VASP proteins in amacrine cells without changing expression levels. We took advantage of a peptide (FP4) known to bind all family members strongly and specifically (Ball et al., 2000; Niebuhr et al., 1997; Zettl and Way, 2002). To achieve uniform distribution, the peptide was targeted to the membrane with a myristoylation sequence, similar to previous experiments *in vitro* (Bear et al., 2000; Lebrand et al., 2004). The peptide was fused to Venus and placed downstream of a floxed stop cassette (*fsf-memVenus-FP4*), enabling visualization of both the distribution of the peptide and the morphology of the transfected cell; *fsf-memVenus* was used as a control. Expression was restricted to late-born amacrine cells by electroporating *Ptf1a-Cre* retinas at P0. Whereas control memVenus-labeled cells developed normal unipolar morphologies (Fig. 9A), the FP4-electroporated amacrine cells exhibited obvious similarities to those in *Fat3* mutants, extending extra processes away from the IPL (Fig. 9B,B′, arrows). Quantification confirmed a significant shift in the distribution of cells with extra neurites (Fig. 9C), as well as a significant increase in the percentage of affected cells in each electroporated region (Fig. 9D). Notably, affected cells typically developed a single extra neurite (Fig. 9B′). Thus, uniform Ena/VASP localization is sufficient to cause formation of ectopic neurites and mimic the *Fat3* mutant phenotype.

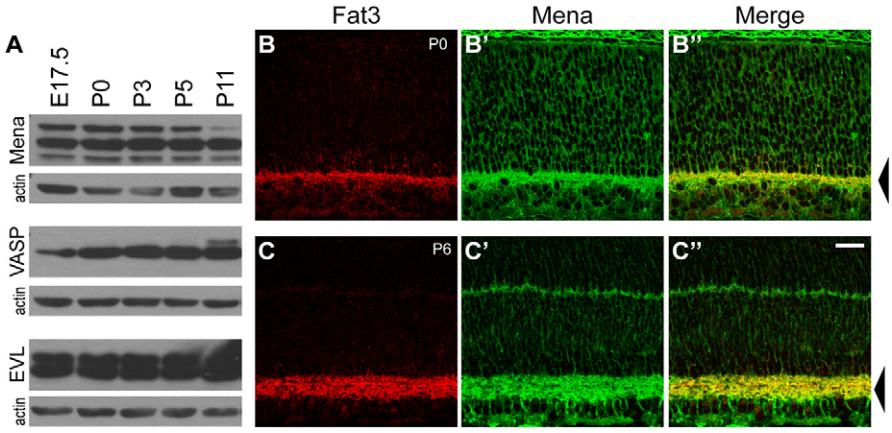

Fig. 6. Fat3 and Ena/VASP proteins are enriched in the IPL throughout retinal development. (A) Western blot analysis confirmed the presence of Mena, VASP and EVL in retinal lysates from E17.5 to P11, which spans amacrine cell development. Actin loading controls are shown underneath each lane. The experiment was performed once using lysates from pools of retinas at each age. (B,C) Immunostaining for Fat3 (red) and Mena (green) confirmed that both proteins are enriched in the IPL (arrowhead) as soon as it forms (P0) and at the end of amacrine cell production (P6). This experiment was performed at least three times with similar results. Scale bar: 30 µm in C″ for B-C″.

Development (2016) 143, 2172-2182 doi:10.1242/dev.133678

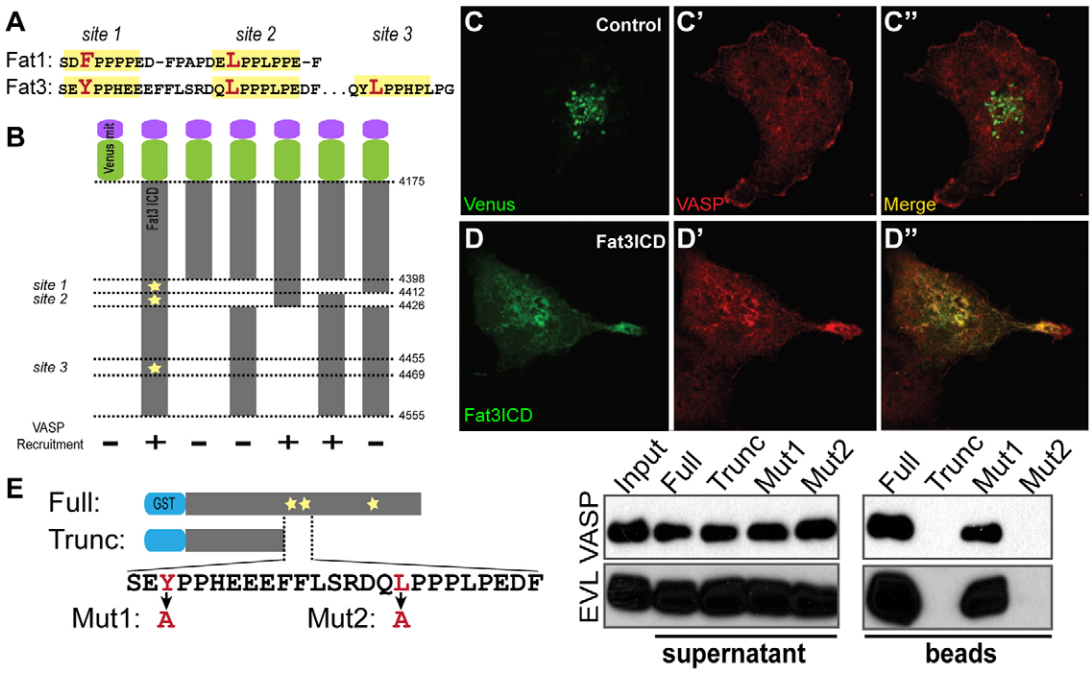

Fig. 7. Fat3 can alter the distribution of Ena/VASP family members through conserved binding sites. (A) Schematic illustrating predicted Ena/VASP binding sites (yellow) aligned in Fat1 and Fat3 intracellular domains (ICD). Residues crucial for binding are highlighted in red. (B) Schematic of proteins targeted to the mitochondria to assay Fat3ICD-Ena/VASP interactions. All proteins were fused to Venus and preceded by a mitochondrial targeting sequence (mit). Yellow stars indicate position of Ena/VASP sites, with amino acids numbered according to the sequence of the full-length protein. At the bottom, each construct's ability to recruit VASP to the mitochondria is indicated. Quantification is shown in Fig. S2. (C-D″) Representative images of COS-7 cells expressing mitVenus alone (green, C,C′) or mitVenus fused to full length Fat3ICD (green, D,D′) and immunostained for endogenous VASP (red, C′,C″,D′,D″). Fat3ICD was sufficient to shift endogenous VASP from the cytoplasm to the mitochondria. (E) GST fusions to full-length Fat3ICD (Full), truncated Fat3ICD (Trunc) or Fat3ICDs harboring point mutations in the first (Mut1) or second (Mut2) predicted binding sites were used to pull down proteins from neonatal brain lysate and analyzed by western blot. Neither VASP nor EVL bound when the second site was mutated. Pulldowns using full-length Fat3ICD were performed three times; truncated Fat3ICD was tested twice; Mut1 and Mut2 were tested once.

DISCUSSION

Although Fat proteins are well-established regulators of tissue polarity, the functions of the Fat-like family remain unclear (Goodrich and Strutt, 2011; Sadeqzadeh et al., 2014). Based on our analysis of Fat3 and its binding partners in retinal amacrine cells, we propose that Fat3 shapes cellular asymmetries by altering the distribution of cytoskeletal effectors such as Ena/VASP proteins. In this model (Fig. 10), the resulting asymmetric distribution of cytoskeletal regulators promotes asymmetric cellular dynamics that are oriented relative to the IPL. In the absence of Fat3, effectors are present more uniformly throughout the cell, including the trailing neurite. As a consequence, there is a loss of asymmetry in the cytoskeleton that disrupts directed migration of the cell body and prevents efficient retraction of the trailing process, which also branches abnormally. Such a mechanism offers an efficient way to link overall changes in cell morphology to the environment.

Our results suggest that Fat3 has an early and general role in amacrine cell morphogenesis. Unlike proteins with subtype-specific functions, Fat3 is enriched throughout the IPL as soon as it is apparent (Deans et al., 2011, Fig. 6). It was therefore peculiar that many *Fat3* mutant amacrine cells achieved correct morphologies, even though multiple subtypes were affected. Our new data show that this late, partially penetrant phenotype is preceded by earlier and broader changes in cell behavior. Additionally, our improved imaging technique revealed that amacrine cells extend leading processes into the IPL as they are migrating, suggesting that asymmetrically localized Fat3 influences generic features of amacrine cell development before they begin to elaborate cell type-specific features. Indeed, in contrast to estimates from fixed tissue, the time-lapse imaging experiments indicated that most *Fat3* mutant cells examined showed changes in cellular dynamics, leading to delayed migration and unreliable retraction of the trailing process. Strikingly, both defects were characterized by a loss of directionality: the cell bodies and the trailing processes moved away from the IPL rather than towards it, and branching was no longer restricted to the leading processes. Taken together, these findings indicate widespread effects that are often resolved, probably due to the compensatory activity of molecules such as the semaphorins (Matsuoka et al., 2011a,b). Thus, the primary function of Fat3 might be to orient the cytoskeleton towards the IPL, during both migration and retraction.

The effects of Fat3 on amacrine cell development are reminiscent of what has been described for N-cadherin elsewhere in the nervous system. N-cadherin is also asymmetrically localized, and this asymmetry precedes the emergence of neuronal polarity in cultured hippocampal neurons (Gärtner et al., 2012, 2015). The activity of N-cadherin is associated with changes in cytoskeletal organization, paralleling the ability of Fat3 to bind to actin regulators. The general effects of both N-cadherin and Fat3 on cell morphology contrast with roles for other receptors involved in dendrite development. For instance, classic cadherins and immunoglobulin domain molecules such as sidekick proteins target neurites to specific lamina in the IPL, but loss of these receptors does not affect overall neuron shape (Duan et al., 2014; Fuerst et al., 2009; Yamagata and Sanes, 2008, 2012). Therefore, asymmetric control of the cytoskeleton by adhesive molecules such as N-cadherin and the Fat-like proteins

Development (2016) 143, 2172-2182 doi:10.1242/dev.133678

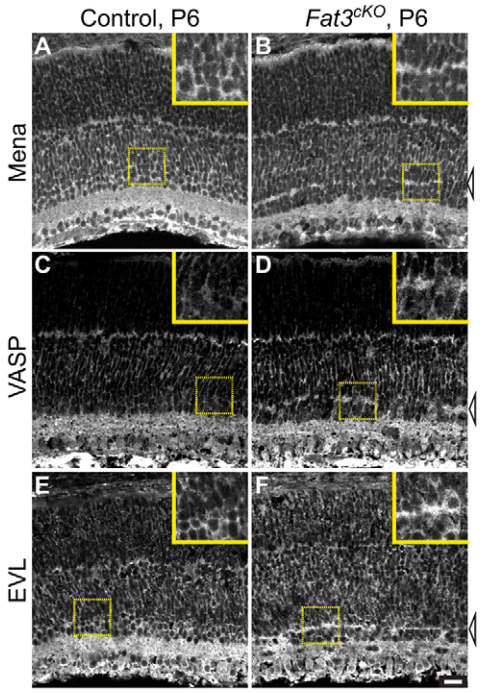

Fig. 8. Loss of Fat3 leads to change in Ena/VASP localization. Immunostaining of Mena (A,B), VASP (C,D) and EVL (E,F) in control (A,C,E) and *Fat3*^{cKO} (B,D,F) retinas at P6. All three are normally enriched in the IPL and are mislocalized in *Fat3* mutants (arrowhead, with magnifications of the boxed areas shown in insets). At least three animals of each genotype were analyzed. Scale bar: 20 µm for main panels and 10 µm for insets.

might provide a novel mechanism for polarizing developing neurons (Solecki, 2012). How Fat3 itself is localized to the leading process remains to be determined; there may be additional signals that break the symmetry of newly born precursors, with Fat3 serving to transmit this information to the cytoskeleton.

Despite their similarity to Fat proteins, Fat-like family members have not been implicated in classic PCP. Hints of less-familiar polarity functions have come from analysis of Fat1, which is required for polarized development and migration of myocytes (Caruso et al., 2013) and cultured fibroblasts (Moeller et al., 2004; Tanoue and Takeichi, 2004). We find that Fat3 exhibits several features expected of a polarity protein. For example, like canonical PCP proteins, Fat3 is asymmetrically localized, in this case to amacrine cell processes in the IPL. Moreover, despite its restricted localization, loss of Fat3 disrupted overall amacrine cell asymmetry from the earliest time points we could visualize. Such global changes suggest that Fat3 normally controls the distribution of actin regulators that can propagate the signal across the cell. In support of this idea, Ena/VASP proteins are bound by Fat3 and enriched with Fat3 in the IPL. Additionally, Ena/VASP protein distribution was altered in *Fat3* mutant retinas. Although such a change could in principle be secondary to the amacrine cell phenotype, our data argue for a causative role, because an FP4-induced change in the distribution of endogenous protein in amacrine cells was sufficient to recapitulate the *Fat3* phenotype. Thus, although Ena/VASP family members are widely expressed, this experiment confirms that they are indeed present in developing amacrine cells and that their proper localization in these cells is essential for normal morphogenesis. These findings are consistent with modeling studies that suggest that even local changes in Ena/VASP activity are sufficient to induce an overall change in cell polarity (Lacayo et al., 2007).

Like Fat proteins, Fat-like proteins contain enormous extracellular domains, which position them to both receive and transmit signals to their neighbors. Our data confirm an autonomous requirement for Fat3, but do not rule out additional non-autonomous functions. Indeed, in *Drosophila*, the effect of Fat-like on actin organization in follicle cells is strictly non-cell autonomous (Viktorinova et al., 2009, 2011). The presence of *Fat3* in retinal ganglion cells underscores the potential for non-autonomous functions, which could explain why migration is more severely affected in *Fat3* null mutants than amacrine cell-specific knockouts (Deans et al., 2011). Whether Fat-like proteins mediate cell-cell interactions by binding to Dachsous family cadherins (Le Pabic et al., 2014; Viktorinova et al., 2009) or instead to each other (Nakayama et al., 2002) remains unclear. Similarly, we still do not know whether such interactions activate a Fat3 signaling pathway or

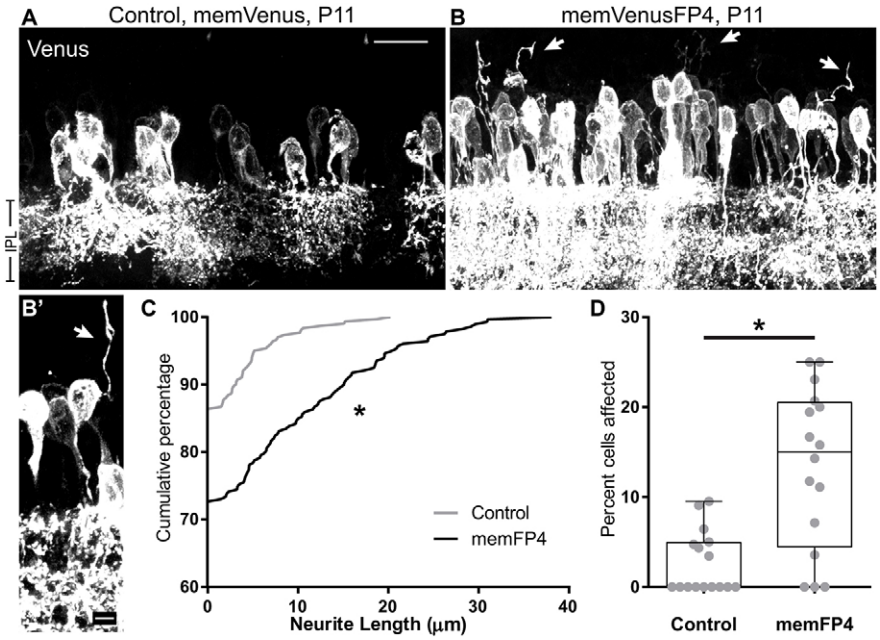

Fig. 9. Redistribution of Ena/VASP is sufficient to recapitulate loss of Fat3. (A,B) Either Venus (control, A) or Venus fused to a strong Ena/VASP family recruitment peptide (memFP4, B) was uniformly targeted to amacrine cell membranes. Expression was restricted to amacrine cells by electroporation of a Cre-dependent construct into *Ptf1a-Cre* pups at P0. Morphology, visualized using Venus, was assessed at P11 and is shown at low (A,B) and high (B′) power. Many extra neurites (arrows) are present in amacrine cells expressing memVenusFP4 (B,B′) but not memVenus (A). Scale bars: 20 µm in A,B and 5 µm in B′. (C) Cumulative histogram of the lengths of all non-IPL facing neurites measured in reconstructions of Cre-electroporated amacrine cells confirms a significant shift in the distribution. **P*=0.0005, Kolmogorov–Smirnov test. (D) Percentage of cells with extra neurites >10 µm in each electroporated region of the retina. Significantly more amacrine cells extended extra neurites in memVenusFP4-electroporated animals compared with controls. *n*=16 electroporated regions from four retinas per condition. *P*=0.0006, Mann–Whitney *U*-test.

Development (2016) 143, 2172-2182 doi:10.1242/dev.133678

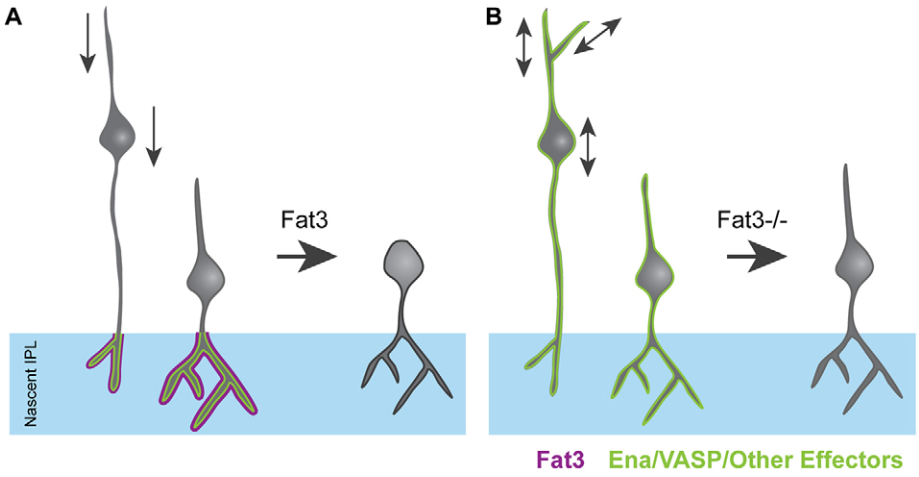

Fig. 10. Our observations suggest a model for Fat3-dependent control of cell morphology. In wild-type amacrine cells (A), Fat3 protein (magenta) is asymmetrically localized to processes in the IPL, biasing the distribution of bound effectors (green). Correspondingly, migration towards the IPL and retraction of the trailing process (arrows) are polarized. Following loss of Fat3 (B), effectors such as Ena/VASP family members are more uniformly distributed. This loss of asymmetry disrupts directed migration and causes the trailing process to act like the leading process, namely failing to retract and branching.

instead serve an adhesive function, for example, localizing Fat3 or securing the Fat3-positive leading process in place.

As more is learned across systems, emerging evidence suggests that Fat-like proteins share the ability to shape the actin cytoskeleton, although the mechanistic details differ. For instance, both Fat1 and Fat3 bind Ena/VASP family proteins, albeit via different sites in the ICD: Fat1 binds through the first putative Ena/VASP binding site (Moeller et al., 2004), Fat3 through the second. Moreover, *Drosophila* Fat-like contains no identifiable Ena/VASP binding sites, but does contain a putative binding site for the WASP family verprolin-homologous protein (WAVE) complex, another major actin regulator. Predicted WAVE complex binding sites are also present in Fat1 and Fat3 (Chen et al., 2014) (our unpublished observation), although again in different regions of the ICD. Indeed, Fat-like ICDs are predicted to bind and therefore coordinate multiple cytoskeletal effectors, making it unlikely that Ena/VASP proteins act alone. Conversely, Ena/VASP proteins have many other roles and are not dedicated to Fat3-mediated functions. Intriguingly, recent genomic mapping studies in humans have linked *FAT1* and *FAT3* to cancer (Katoh, 2012; Sadeqzadeh et al., 2014) and *FAT1* to autism (Cukier et al., 2014; Neale et al., 2012). Dysregulation of cell shape could enhance metastasis, whereas alterations in neuronal shape and hence connectivity, as observed in the retina, could contribute to the etiology of autism. Thus, Fat-like regulation of the cytoskeleton might offer a satisfying explanation for the roles of Fat-like genes in seemingly disparate diseases.

MATERIALS AND METHODS

Animals

The following mouse strains were used: floxed *Fat3* (*Fat3*$^{fl/fl}$) and null *Fat3* (*Fat3*$^{+/-}$) (Deans et al., 2011), *Ptf1a-Cre* (Kawaguchi et al., 2002) and *AI14 Rosa26-tdTomato* (Madisen et al., 2010). Mice of either sex were used, with a mixed background including C57Bl6, 129SV/J, and CD1. Protocols were approved by the Institutional Animal Use Care Committee at Harvard Medical School.

Antibodies

Antibodies used were: mouse anti-Mena (Lanier et al., 1999; Lebrand et al., 2004), rabbit anti-Mena (#2197) (Bear et al., 2000; Lambrechts et al., 2000; Lanier et al., 1999), anti-VASP (#2010) (Bear et al., 2000; Menzies et al., 2004), anti-EVL (#1404) (Lambrechts et al., 2000), anti-Fat3 (Deans et al., 2011), anti-actin (Abcam, 28226) and anti-DsRed (Clontech, 632496) to enhance tdTomato. Mena, VASP and EVL antibodies were a gift from Frank Gertler (Massachusetts Institute of Technology). Antibody performance was consistent across experiments and matched published descriptions (see supplementary Materials and Methods for further details).

In vivo retinal electroporation, imaging and analysis

Retinal electroporations were performed as described (Matsuda and Cepko, 2004). Retinas were collected at P11, enucleated and fixed in 4% paraformaldehyde (PFA) at 4°C overnight, cryoprotected in 30% sucrose, (Thermo-Scientific), then flash frozen in NEG-50 (Thermo-Scientific). Retinas were cryosectioned at 40 µm and imaged blind to condition with an Olympus FV1200 confocal microscope (see supplementary Materials and Methods for further details). Amira software (FEI) was used to create and analyze isosurface three-dimensional reconstructions of amacrine cells in stacks taken from four independent regions of 4 retinas per condition.

Late-born amacrine cells were labeled by electroporation with *CAG-fsf-memVenus* and *CAG-fsf-mitVenus* at P0 (Fig. 1). Analysis, blind to condition, was limited to cells positioned below the extra plexiform layer. To assess cell autonomy (Fig. 5), *CAG-fsf-memVenus*, *Ndrg4-Cre* and *Ndrg4-tdTomato* or *Ndrg4-tdTomatoNLS* were co-electroporated. Expression of tdTomato and morphology were used to confirm amacrine cell identity. To assess the role of Ena/VASP distribution (Fig. 9), *CAG-fsf-memVenus* or *CAG-fsf-memVenusFP4* were electroporated. In all cases, all neurites extending outside of the IPL were measured in three-dimensional reconstructions using Amira software.

CAG-fsf-memVenus and *CAG-fsf-memVenusFP4* were created by inserting *memVenus* or *GFP-FPPPx4-CAAX* (Bear et al., 2000) modified to express Venus instead of GFP into the vector backbone from *CAG-loxP-stop-loxP-GFP* (Addgene plasmid #13769) (Matsuda and Cepko, 2004). The *Ndrg4-Cre* construct was a gift from Constance Cepko (Harvard Medical School), and shares a backbone with Addgene plasmid #13766 (Matsuda and Cepko, 2004). *Ndrg4-tdTomato* and *Ndrg4-tdTomatoNLS* were created using the same *Ndrg4* backbone with a *tdTomato* or *tdTomatoNLS* insert. All constructs were verified by sequencing.

Ex vivo retinal electroporation and live imaging

P0 retinas were dissected from *Ptf1a-Cre* pups, electroporated with *CAG-fsf-tdTomato* and *CAG-fsf-mNeonGreen-GM130* (Matsuda and Cepko, 2004) and prepared as described (Surzenko et al., 2013). Amacrine cells were imaged using a Zeiss 710 NLO multiphoton microscope with an environmental chamber (see supplementary Materials and Methods). The mTrackJ plugin in ImageJ (NIH) was used to track the center of the cell body and trailing tip manually in each frame. The branching index was calculated by counting the number of branches in each frame of time-lapse image series and dividing by the total frame number.

Retina immunostaining and imaging

Retinas were collected at P0, P1, P6, or P11 and processed as above. Cryosections (14-20 µm) were stained with rabbit anti-Fat3 (1:500), mouse anti-pan-Mena (1:300), rabbit anti-Mena #2197 (1:250), rabbit anti-VASP #2010 (1:250), anti-EVL #1404 (1:500) and/or rabbit anti-Dsred (1:1000). Images were collected using an Olympus FV1200 confocal microscope (see supplementary Materials and Methods). To quantify cell distribution, ImageJ was used to measure the position of labeled cells with respect to the

Development (2016) 143, 2172-2182 doi:10.1242/dev.133678

upper and lower limits of the INL in four different regions of four retinas of each genotype. The percentage of distance to the IPL traveled was calculated in Excel using these measurements.

Mitochondrial recruitment assay

COS-7 cells (Goodrich laboratory stock supply) were transfected with Lipofectamine 2000 (Invitrogen) with equal concentrations of mitochondrial-targeted Fat3ICD constructs (see Fig. 7). After 24 h, cells were fixed with 4% paraformaldehyde (PFA) for 20 min and stained with anti-VASP (1:750). Cells were imaged using an Olympus FV1000 laser-scanning confocal microscope. Colocalization was quantified using the coloc2 plugin in ImageJ (NIH).

The N-terminal mitochondrial targeting tag MVGRNSAIAAGVCGA-LFIGYCIYFDRKRRGDPN from Tom20 (Kanaji et al., 2000) was inserted upstream of *Venus* or *Venus* fused to a *Fat3ICD* fragment. Full-length Fat3ICD spanned from amino acid (aa) 4175 to 4555, numbered according to UniProt Q8BNA6. Constructs used to map interaction sites were: *Truncation 1*, aa4175-4398; *Deletion 1,2*, aa4175-4398, 4426-4555; *Truncation 2*, aa4175-4427; *Deletion 1*, aa4175-4398, 4412-4555; and *Deletion 2*, aa4175-4411, 4426-4555.

Pulldown assays

GST-Fat3ICD fusion proteins were grown in Rosetta *E. coli* (Millipore) and bound to glutathione Sepharose beads (GE Life Sciences). Beads were used for pulldowns from P1 retina lysate (see supplementary Materials and Methods for further details), followed by western blot analysis using standard methods.

Western blots

Standard western blotting protocols were followed using rabbit anti-Mena #2197 (1:5000), anti-VASP #2010 (1:5000) and anti-EVL #1404 (1:5000). To control for loading, blots were stripped (Thermoscientific Product 2105) and reprobed with anti-actin (1:10,000). All proteins migrated at expected molecular mass. Uncropped images are available on request.

Statistics

Sample sizes were determined by performing small pilot studies or based on prior experience analyzing similar biological effects. Animals of appropriate genotypes were assigned to experimental groups randomly, as available. Damaged or unhealthy tissue was excluded from analysis, based on qualitative assessment. Electroporation experiments were performed blind to genotype, but with known DNA constructs. Imaging and analysis were performed on randomized samples, blind to genotype and treatment. Statistical tests were chosen in consultation with a biostatistician (Emanuele Mazzola, Dana-Farber Cancer Institute) and performed using Prism software (GraphPad). Non-parametric tests were used because the data were often not normally distributed; all individual data points are shown. For comparisons between two groups, a Mann–Whitney *U*-test was used, except for cumulative distributions, where a Kolmogorov–Smirnov test was used and Fig. 3C, where a Student's *t*-test was used because of small sample size. To test significance among multiple groups (Fig. S2), a one-way ANOVA with Bonferroni multiple comparison correction was used.

Acknowledgements

We thank the Neurobiology Department and the Neurobiology Imaging Facility for consultation and instrument availability that supported this work. We are grateful to F. Gertler for sharing of reagents and helpful advice, as well as C. Cepko and lab for generous sharing of confocal equipment, reagents and guidance, particularly N. Surzenko for assistance with live imaging and T. Cherry with retinal electroporation. We also thank E. Mazzola and S. Ursprung for help with statistics.

Competing interests

The authors declare no competing or financial interests.

Author contributions

A.K. and L.V.G. conceived the project. A.K., S.J.H. and L.V.G. designed and interpreted experiments. A.K. and S.J.H. performed experiments. A.K. and L.V.G. wrote the manuscript, with significant input from S.J.H.

Funding

This work was supported by the National Eye Institute [R21 EY022725 to L.V.G. and F32 EY024184 to S.H.]; the National Institute of Neurological Disorders and Stroke [T32 NS007484 to S.J.H.]; and graduate research fellowships from the National Science Foundation and Stuart H.Q. and Victoria Quan (to A.K.). We also benefited from the use of the Neurobiology Imaging Facility which is supported by the National Institute of Neurological Disorders and Stroke [P30 NS072030]. Deposited in PMC for release after 12 months.

Supplementary information

Supplementary information available online at
http://dev.biologists.org/lookup/suppl/doi:10.1242/dev.133678/-/DC1

References

Ball, L. J., Kühne, R., Hoffmann, B., Häfner, A., Schmieder, P., Volkmer-Engert, R., Hof, M., Wahl, M., Schneider-Mergener, J., Walter, U. et al. (2000). Dual epitope recognition by the VASP EVH1 domain modulates polyproline ligand specificity and binding affinity. *EMBO J.* **19**, 4903-4914.

Barnes, A. P., Solecki, D. and Polleux, F. (2008). New insights into the molecular mechanisms specifying neuronal polarity in vivo. *Curr. Opin. Neurobiol.* **18**, 44-52.

Bear, J. E. and Gertler, F. B. (2009). Ena/VASP: towards resolving a pointed controversy at the barbed end. *J. Cell Sci.* **122**, 1947-1953.

Bear, J. E., Loureiro, J. J., Libova, I., Fässler, R., Wehland, J. and Gertler, F. B. (2000). Negative regulation of fibroblast motility by Ena/VASP proteins. *Cell* **101**, 717-728.

Caruso, N., Herberth, B., Bartoli, M., Puppo, F., Dumonceaux, J., Zimmermann, A., Denadai, S., Lebosse, M., Roche, S., Geng, L. et al. (2013). Deregulation of the protocadherin gene FAT1 alters muscle shapes: implications for the pathogenesis of facioscapulohumeral dystrophy. *PLoS Genet.* **9**, e1003550.

Chen, B., Brinkmann, K., Chen, Z., Pak, C. W., Liao, Y., Shi, S., Henry, L., Grishin, N. V., Bogdan, S. and Rosen, M. K. (2014). The WAVE regulatory complex links diverse receptors to the actin cytoskeleton. *Cell* **156**, 195-207.

Cherry, T. J., Trimarchi, J. M., Stadler, M. B. and Cepko, C. L. (2009). Development and diversification of retinal amacrine interneurons at single cell resolution. *Proc. Natl. Acad. Sci. USA* **106**, 9495-9500.

Cukier, H. N., Dueker, N. D., Slifer, S. H., Lee, J. M., Whitehead, P. L., Lalanne, E., Leyva, N., Konidari, I., Gentry, R. C., Hulme, W. F. et al. (2014). Exome sequencing of extended families with autism reveals genes shared across neurodevelopmental and neuropsychiatric disorders. *Mol. Autism* **5**, 1.

Deans, M. R., Krol, A., Abraira, V. E., Copley, C. O., Tucker, A. F. and Goodrich, L. V. (2011). Control of neuronal morphology by the atypical cadherin fat3. *Neuron* **71**, 820-832.

Dent, E. W., Kwiatkowski, A. V., Mebane, L. M., Philippar, U., Barzik, M., Rubinson, D. A., Gupton, S., Van Veen, J. E., Furman, C., Zhang, J. et al. (2007). Filopodia are required for cortical neurite initiation. *Nat. Cell Biol.* **9**, 1347-1359.

Devenport, D. (2014). The cell biology of planar cell polarity. *J. Cell Biol.* **207**, 171-179.

Duan, X., Krishnaswamy, A., De la Huerta, I. and Sanes, J. R. (2014). Type II cadherins guide assembly of a direction-selective retinal circuit. *Cell* **158**, 793-807.

Fanto, M., Clayton, L., Meredith, J., Hardiman, K., Charroux, B., Kerridge, S. and McNeill, H. (2003). The tumor-suppressor and cell adhesion molecule Fat controls planar polarity via physical interactions with Atrophin, a transcriptional co-repressor. *Development* **130**, 763-774.

Fuerst, P. G., Bruce, F., Tian, M., Wei, W., Elstrott, J., Feller, M. B., Erskine, L., Singer, J. H. and Burgess, R. W. (2009). DSCAM and DSCAML1 function in self-avoidance in multiple cell types in the developing mouse retina. *Neuron* **64**, 484-497.

Gärtner, A., Fornasiero, E. F. and Dotti, C. G. (2012). N-cadherin: a new player in neuronal polarity. *Cell Cycle* **11**, 2223-2224.

Gärtner, A., Fornasiero, E. F. and Dotti, C. G. (2015). Cadherins as regulators of neuronal polarity. *Cell Adh. Migr.* **9**, 4409-4419.

Goh, K. L., Cai, L., Cepko, C. L. and Gertler, F. B. (2002). Ena/VASP proteins regulate cortical neuronal positioning. *Curr. Biol.* **12**, 565-569.

Goodrich, L. V. and Strutt, D. (2011). Principles of planar polarity in animal development. *Development* **138**, 1877-1892.

Harumoto, T., Ito, M., Shimada, Y., Kobayashi, T. J., Ueda, H. R., Lu, B. and Uemura, T. (2010). Atypical cadherins Dachsous and Fat control dynamics of noncentrosomal microtubules in planar cell polarity. *Dev. Cell* **19**, 389-401.

Hinds, J. W. and Hinds, P. L. (1978). Early development of amacrine cells in the mouse retina: an electron microscopic, serial section analysis. *J. Comp. Neurol.* **179**, 277-300.

Hinds, J. W. and Hinds, P. L. (1983). Development of retinal amacrine cells in the mouse embryo: evidence for two modes of formation. *J. Comp. Neurol.* **213**, 1-23.

Kanaji, S., Iwahashi, J., Kida, Y., Sakaguchi, M. and Mihara, K. (2000). Characterization of the signal that directs Tom20 to the mitochondrial outer membrane. *J. Cell Biol.* **151**, 277-288.

Katoh, M. (2012). Function and cancer genomics of FAT family genes (review). *Int. J. Oncol.* **41**, 1913-1918.
Kawaguchi, Y., Cooper, B., Gannon, M., Ray, M., MacDonald, R. J. and Wright, C. V. E. (2002). The role of the transcriptional regulator Ptf1a in converting intestinal to pancreatic progenitors. *Nat. Genet.* **32**, 128-134.
Krause, M., Dent, E. W., Bear, J. E., Loureiro, J. J. and Gertler, F. B. (2003). Ena/VASP proteins: regulators of the actin cytoskeleton and cell migration. *Annu. Rev. Cell Dev. Biol.* **19**, 541-564.
Kwiatkowski, A. V., Rubinson, D. A., Dent, E. W., Edward van Veen, J., Leslie, J. D., Zhang, J., Mebane, L. M., Philippar, U., Pinheiro, E. M., Burds, A. A. et al. (2007). Ena/VASP is required for neuritogenesis in the developing cortex. *Neuron* **56**, 441-455.
Lacayo, C. I., Pincus, Z., VanDuijn, M. M., Wilson, C. A., Fletcher, D. A., Gertler, F. B., Mogilner, A. and Theriot, J. A. (2007). Emergence of large-scale cell morphology and movement from local actin filament growth dynamics. *PLoS Biol.* **5**, e233.
Lambrechts, A., Kwiatkowski, A. V., Lanier, L. M., Bear, J. E., Vandekerckhove, J., Ampe, C. and Gertler, F. B. (2000). cAMP-dependent protein kinase phosphorylation of EVL, a Mena/VASP relative, regulates its interaction with actin and SH3 domains. *J. Biol. Chem.* **275**, 36143-36151.
Lanier, L. M., Gates, M. A., Witke, W., Menzies, A. S., Wehman, A. M., Macklis, J. D., Kwiatkowski, D., Soriano, P. and Gertler, F. B. (1999). Mena is required for neurulation and commissure formation. *Neuron* **22**, 313-325.
Le Pabic, P., Ng, C. and Schilling, T. F. (2014). Fat-Dachsous signaling coordinates cartilage differentiation and polarity during craniofacial development. *PLoS Genet.* **10**, e1004726.
Lebrand, C., Dent, E. W., Strasser, G. A., Lanier, L. M., Krause, M., Svitkina, T. M., Borisy, G. G. and Gertler, F. B. (2004). Critical role of Ena/VASP proteins for filopodia formation in neurons and in function downstream of netrin-1. *Neuron* **42**, 37-49.
Madisen, L., Zwingman, T. A., Sunkin, S. M., Oh, S. W., Zariwala, H. A., Gu, H., Ng, L. L., Palmiter, R. D., Hawrylycz, M. J., Jones, A. R. et al. (2010). A robust and high-throughput Cre reporting and characterization system for the whole mouse brain. *Nat. Neurosci.* **13**, 133-140.
Matis, M., Russler-Germain, D. A., Hu, Q., Tomlin, C. J. and Axelrod, J. D. (2014). Microtubules provide directional information for core PCP function. *Elife* **3**, e02893.
Matsuda, T. and Cepko, C. L. (2004). Electroporation and RNA interference in the rodent retina in vivo and in vitro. *Proc. Natl. Acad. Sci. USA* **101**, 16-22.
Matsuoka, R. L., Chivatakarn, O., Badea, T. C., Samuels, I. S., Cahill, H., Katayama, K.-I., Kumar, S. R., Suto, F., Chédotal, A., Peachey, N. S. et al. (2011a). Class 5 transmembrane semaphorins control selective Mammalian retinal lamination and function. *Neuron* **71**, 460-473.
Matsuoka, R. L., Nguyen-Ba-Charvet, K. T., Parray, A., Badea, T. C., Chédotal, A. and Kolodkin, A. L. (2011b). Transmembrane semaphorin signalling controls laminar stratification in the mammalian retina. *Nature* **470**, 259-263.
Menzies, A. S., Aszodi, A., Williams, S. E., Pfeifer, A., Wehman, A. M., Goh, K. L., Mason, C. A., Fassler, R. and Gertler, F. B. (2004). Mena and vasodilator-stimulated phosphoprotein are required for multiple actin-dependent processes that shape the vertebrate nervous system. *J. Neurosci.* **24**, 8029-8038.
Moeller, M. J., Soofi, A., Braun, G. S., Li, X., Watzl, C., Kriz, W. and Holzman, L. B. (2004). Protocadherin FAT1 binds Ena/VASP proteins and is necessary for actin dynamics and cell polarization. *EMBO J.* **23**, 3769-3779.
Nakayama, M., Nakajima, D., Yoshimura, R., Endo, Y. and Ohara, O. (2002). MEGF1/fat2 proteins containing extraordinarily large extracellular domains are localized to thin parallel fibers of cerebellar granule cells. *Mol. Cell. Neurosci.* **20**, 563-578.
Neale, B. M., Kou, Y., Liu, L., Ma'ayan, A., Samocha, K. E., Sabo, A., Lin, C.-F., Stevens, C., Wang, L.-S., Makarov, V. et al. (2012). Patterns and rates of exonic de novo mutations in autism spectrum disorders. *Nature* **485**, 242-245.
Niebuhr, K., Ebel, F., Frank, R., Reinhard, M., Domann, E., Carl, U. D., Walter, U., Gertler, F. B., Wehland, J. and Chakraborty, T. (1997). A novel proline-rich motif present in ActA of Listeria monocytogenes and cytoskeletal proteins is the ligand for the EVH1 domain, a protein module present in the Ena/VASP family. *EMBO J.* **16**, 5433-5444.
Saburi, S., Hester, I., Fischer, E., Pontoglio, M., Eremina, V., Gessler, M., Quaggin, S. E., Harrison, R., Mount, R. and McNeill, H. (2008). Loss of Fat4 disrupts PCP signaling and oriented cell division and leads to cystic kidney disease. *Nat. Genet.* **40**, 1010-1015.
Saburi, S., Hester, I., Goodrich, L. and McNeill, H. (2012). Functional interactions between Fat family cadherins in tissue morphogenesis and planar polarity. *Development* **139**, 1806-1820.
Sadeqzadeh, E., de Bock, C. E. and Thorne, R. F. (2014). Sleeping giants: emerging roles for the fat cadherins in health and disease. *Med. Res. Rev.* **34**, 190-221.
Solecki, D. J. (2012). Sticky situations: recent advances in control of cell adhesion during neuronal migration. *Curr. Opin. Neurobiol.* **22**, 791-798.
Sopko, R. and McNeill, H. (2009). The skinny on Fat: an enormous cadherin that regulates cell adhesion, tissue growth, and planar cell polarity. *Curr. Opin. Cell Biol.* **21**, 717-723.
Surzenko, N., Crowl, T., Bachleda, A., Langer, L. and Pevny, L. (2013). SOX2 maintains the quiescent progenitor cell state of postnatal retinal Muller glia. *Development* **140**, 1445-1456.
Tanoue, T. and Takeichi, M. (2004). Mammalian Fat1 cadherin regulates actin dynamics and cell-cell contact. *J. Cell Biol.* **165**, 517-528.
Tanoue, T. and Takeichi, M. (2005). New insights into Fat cadherins. *J. Cell Sci.* **118**, 2347-2353.
Viktorinova, I., Konig, T., Schlichting, K. and Dahmann, C. (2009). The cadherin Fat2 is required for planar cell polarity in the Drosophila ovary. *Development* **136**, 4123-4132.
Viktorinova, I., Pismen, L. M., Aigouy, B. and Dahmann, C. (2011). Modelling planar polarity of epithelia: the role of signal relay in collective cell polarization. *J. R. Soc. Interface* **8**, 1059-1063.
Voinescu, P. E., Kay, J. N. and Sanes, J. R. (2009). Birthdays of retinal amacrine cell subtypes are systematically related to their molecular identity and soma position. *J. Comp. Neurol.* **517**, 737-750.
Yamagata, M. and Sanes, J. R. (2008). Dscam and Sidekick proteins direct lamina-specific synaptic connections in vertebrate retina. *Nature* **451**, 465-469.
Yamagata, M. and Sanes, J. R. (2012). Expanding the Ig superfamily code for laminar specificity in retina: expression and role of contactins. *J. Neurosci.* **32**, 14402-14414.
Zettl, M. and Way, M. (2002). The WH1 and EVH1 domains of WASP and Ena/VASP family members bind distinct sequence motifs. *Curr. Biol.* **12**, 1617-1622.